Letter

QMC-consistent static spin and density local field factors for the uniform electron gas

Aaron D. Kaplan *
Department of Physics, Temple University, Philadelphia, Pennsylvania 19122, USA

Carl A. Kukkonen †
33841 Mercator Isle, Dana Point, California 92629, USA

(Received 15 March 2023; accepted 17 May 2023; published 30 May 2023)

Analytic mathematical models for the static spin (G_-) and density (G_+) local field factors for the uniform electron gas (UEG) as functions of wave vector and density are presented. These models closely fit recent quantum Monte Carlo (QMC) data and satisfy exact asymptotic limits. A simple functional form for G_- is developed; the same functional form parametrized for G_+ yields an improvement over previous work. The QMC-computed $G_\pm$ are consistent with a rapid crossover between theoretically derived small-q and large-q expansions of $G_\pm$. These expansions are completely determined by r_s, the UEG correlation energy per electron, and the UEG on-top pair distribution function. We demonstrate their utility by computing uniform electron gas correlation energies over a range of densities. These models, which hold over an extremely wide range of densities, are recommended for use in practical time-dependent density functional theory calculations of simple metallic systems. A revised model of the spin susceptibility enhancement is developed that fits QMC data, and does not show a ferromagnetic instability at low density.

DOI: 10.1103/PhysRevB.107.L201120

A critical quantity for evaluating the linear response of an interacting uniform electron gas (UEG), or simple metal, are the local field factors (LFFs) $G_\pm(r_s, q, \omega)$. The UEG (sometimes called jellium) can be characterized by a Wigner-Seitz density parameter $r_s = [3/(4\pi n)]^{1/3}$ and relative spin polarization $\zeta = (n_\uparrow - n_\downarrow)/n$, for total density $n = n_\uparrow + n_\downarrow$. The density (spin-symmetric) LFF $G_+(r_s, q, \omega)$ governs the density-density response $\chi(q, \omega)$ of a many-electron density to a wave vector q- and frequency ω-dependent perturbation via [1]

$$\chi^{-1}(q, \omega) = \chi_0^{-1}(q, \omega) - \frac{4\pi}{q^2}[1 - G_+(r_s, q, \omega)]. \quad (1)$$

$\chi_0(q, \omega)$ is the response function of noninteraction electrons; for the UEG, this is the Lindhard function [2]. Thus G_+ is related to the exchange-correlation kernel f_{xc} of time-dependent density functional theory (TD-DFT) [3,4] as $G_+(r_s, q, \omega) = -q^2 f_{xc}(r_s, q, \omega)/(4\pi)$. The spin (antisymmetric) LFF governs the paramagnetic spin response via [1]

$$\chi_{S_zS_z}^{-1}(q, \omega) = \chi_0^{-1}(q, \omega) + \frac{4\pi}{q^2} G_-(r_s, q, \omega). \quad (2)$$

There exist many approximate expressions of G_+ or f_{xc}, which range from those which are local in space and time [5], nonlocal in space only (as in this work) [6,7], nonlocal in time only [4,8], or nonlocal in both space and time [9–11]. However, there are no *realistic* expressions of G_- other than that of Richardson and Ashcroft (RA) [9], which is based on perturbation theory calculations, and is complicated by typographical errors. As we make extensive comparisons to the RA LFFs, we correct these typographical errors in Supplemental Material [12] Sec. S6. The RA LFFs are presumably most realistic at higher densities typical of simple metals, and less realistic at lower densities.

This Letter provides flexible, analytic expressions for the static LFFs $G_\pm(r_s, q) \equiv \lim_{\omega\to 0} G_\pm(r_s, q, \omega)$ based on known asymptotic limits. Free parameters are then fitted to recent variational diagrammatic quantum Monte Carlo (QMC) calculations [13]. This QMC data covers the region below $q = 2.34k_F$ for $r_s = 1$–5 for G_-, but is only available for $r_s = 1$ and 2 for G_+. The current model of $G_+(r_s, q)$ also more reliably fits older QMC data [14] that covers $r_s = 2$, 5, and 10, but with no data below k_F, than the expression due to Corradini *et al.* [7], and provides accurate predictions of the UEG correlation energy.

Both $G_\pm(r_s, q)$ are characterized by a rapid crossover between small- and large-q asymptotics near $q = 2k_F$, with $k_F = (3\pi^2 n)^{1/3}$ the Fermi wave vector. This crossover is likely responsible for the "$2k_F$-hump" phenomenon [15,16]: A maximum in $G_+(q)$ may exist for $q \approx 2k_F$. The presence of a peak can markedly change the properties of phonon dispersion [17], superconducting critical temperatures [18], etc., when using $G_+(q)$ to approximate the LFF of simple metals in TD-DFT. Moreover, explicit inclusion of the spin dependence of the electronic response via G_- is crucial for describing, for example, pairing of electrons in superconducting phases [19,20]. Thus a realistic approximation of G_- at all possible densities and wave vectors is needed to understand the spin dependence of the electronic response. Such a model G_-

*Present address: Lawrence Berkeley National Laboratory, Berkeley, CA 94720; ADKaplan@lbl.gov
†kukkonen@cox.net

would enable realistic calculations of simple metals using the Kukkonen-Overhauser framework [19] or other theories of linear response.

In this Letter, we present the formulas for G_+ and G_- for all wave vectors given only the density r_s. The details of the curve fitting, asymptotic behavior, and code are given in the Supplemental Material [12] (see also Refs. [21–24] therein). The formulas may look complex, but are simple to implement computationally; a documented PYTHON implementation is provided in the public code repository [25]. More, the models with optimized parameters can be accessed from PyPI by pip installing "AKCK_LFF."

The QMC data for both G_+ and G_- closely follow the theoretical asymptotic behavior of varying as q^2 at small q. The coefficients of q^2 are determined by the compressibility and susceptibility sum rules. The QMC data rise somewhat faster than q^2 to about $2k_F$, and then fall rapidly. Theory predicts that the large-q behavior of $G_\pm$ is $B_\pm + Cq^2$. Although B_+ and B_- differ, they are determined by r_s and the on-top pair correlation function. C is the same for both $G_\pm$. The qualitatively similar behaviors of the LFFs permit us to use the same analytically simple expressions, defined below in Eqs. (3) and (4), to model G_+ and G_-.

The fitting process, partially described below, simply allows the small-q behavior to rise above q^2, combined with an adjustable exponential cutoff near $2k_F$. This cutoff modulates the transition to the large q asymptotics. The recent QMC data stops at $2.34k_F$, but is consistent with the large-q asymptotic behavior, assuming a simple transition. The following equations completely specify the local field factors.

Let $x \equiv q/k_F$, then we model *both* $G_\pm$ as

$$G_j(r_s, q) = x^2[A_j(r_s) + \alpha_j(r_s)x^4]H(x^4/16; a_{3j}, a_{4j}) + [C(r_s)x^2 + B_j(r_s)][1 - H(x^4/16; a_{3j}, a_{4j})], \tag{3}$$

$$\alpha_j(r_s) = a_{0j} + a_{1j}\exp(-a_{2j}r_s), \tag{4}$$

where $j = +, -$. The smoothed step function

$$H(y; \beta, \gamma) = \frac{(e^{\beta\gamma} - 1)e^{-\beta y}}{1 + (e^{\beta\gamma} - 2)e^{-\beta y}} \tag{5}$$

is constructed to satisfy three limits: $H(0; \beta, \gamma) = 1$, $H(\gamma; \beta, \gamma) = 1/2$, and $H(\infty; \beta, \gamma) = 0$. While H has no physical basis, it represents a simple and reasonable transition from the low-q behavior of the QMC data to the large-q asymptotics. The a_{ij} parameters are fitted to QMC data.

Equation (3) satisfies the exact small-q expansions (SQEs) of $G_\pm$, which are identical in structure. For G_+, this is the compressibility sum rule,

$$\lim_{q\to 0} G_+(r_s, q) = A_+(r_s)x^2 + O(x^4), \tag{6}$$

$$A_+(r_s) = -\frac{k_F^2}{4\pi}\frac{\partial^2 e_{xc}^{LDA}}{\partial n^2}(r_s), \tag{7}$$

with e_{xc}^{LDA} the local-density approximation [26–28] for the UEG exchange-correlation energy density. Unless specified, we use hartree atomic units, $\hbar = m_e = e^2 = 1$; 1 hartree energy unit is 2 Ry, or 27.211 386 eV; 1 bohr length unit is 0.529 177 Å [29]. The SQE of G_- is the susceptibility sum rule [1]:

$$\lim_{q\to 0} G_-(r_s, q) = A_-(r_s)x^2 + O(x^4), \tag{8}$$

$$A_-(r_s) = -\frac{3\pi}{4k_F}\frac{\partial^2 \varepsilon_{xc}^{LSDA}}{\partial \zeta^2}(r_s, 0). \tag{9}$$

For simple polynomial approximations of $A_\pm(r_s)$ valid for $1 \leqslant r_s \leqslant 5$, see Eqs. (6) and (7) of Ref. [13]. ε_{xc}^{LSDA} is the local spin-density approximation for the UEG exchange-correlation energy per electron, for which we use the Perdew-Wang approximation (PW92) [28]. The quantity

$$\alpha_{xc}(r_s) \equiv \frac{\partial^2 \varepsilon_{xc}^{LSDA}}{\partial \zeta^2}(r_s, 0) \tag{10}$$

is often called the spin stiffness [30]. The exchange contribution to the spin stiffness can be shown to be $\alpha_x(r_s) = -k_F/(3\pi)$ [26,27,31].

Equation (3) also satisfies the large-q expansions (LQEs) of $G_\pm$, again identical in structure. For G_+ [7],

$$\lim_{q\to\infty} G_+(r_s, q) = C(r_s)x^2 + B_+(r_s) + O(x^{-2}), \tag{11}$$

$$C(r_s) = -\frac{\pi}{2k_F}\frac{\partial}{\partial r_s}\left[r_s\varepsilon_c^{LDA}(r_s)\right]. \tag{12}$$

The function $B_+(r_s)$ is parametrized as [14]

$$B_+(r_s) = \frac{1 + (2.15)r_s^{1/2} + (0.435)r_s^{3/2}}{3 + (1.57)r_s^{1/2} + (0.409)r_s^{3/2}}. \tag{13}$$

The LQEs of G_- and G_+ are connected as [1,9,32,33]

$$\lim_{q\to\infty} G_-(r_s, q) = C(r_s)x^2 + B_-(r_s) + O(x^{-2}), \tag{14}$$

$$B_-(r_s) = B_+(r_s) + 2g(r_s) - 1, \tag{15}$$

i.e., they differ only by the on-top pair distribution function $g(r_s)$, which we approximate as [34]

$$g(r_s) = \frac{1}{2}\frac{1 + 2(0.193)r_s}{\{1 + (0.525)r_s[1 + (0.193)r_s]\}^2}. \tag{16}$$

To fit Eq. (3) for $G_\pm$, we minimize the deviation from the QMC-computed values of $G_\pm$, weighted by their corresponding uncertainties. The fitting method is described fully in Supplemental Material Sec. S1. Table I presents fitted parameters a_{ij} and their uncertainties estimated using a bootstrap method. This method is described in Supplemental Material Sec. S1. We recommend using the full precision of the parameters rather than truncated values based on uncertainty estimates.

Figure 1 compares our fitted G_+ to the data of Ref. [13] and to the older QMC data of Moroni *et al.* [14] for $r_s = 2$. The quality of fit is excellent, lying within the uncertainty of the QMC data at all computed points. The LFF of Corradini *et al.* [7], although fitted to the Moroni *et al.* data, fits it poorly. The LFF developed here, fitted to the Moroni *et al.* data at $r_s = 5$ and 10 only, fits it rather well.

The Supplemental Material presents further plots of G_+ that demonstrate the quality of fit to the data of Refs. [13,14] in Figs. S1–S3. Supplemental Figs. S8 and S9 show that our model realistically extrapolates to values of r_s for which there are no QMC data. For surface plots of G_+ at metallic densities,

TABLE I. Fit parameters a_{ij} for the model LFFs of Eq. (3) and the estimated uncertainties in the parameters. $i = 0, 1, 2, 3, 4$, and $j = +$ for the G_+ parameters, and $j = -$ for the G_- parameters. The rightmost column uses a revised parametrization for the correlation spin stiffness, described below. Only a_{0-} is sensitive to the choice of α_c, although that may be due to its relatively larger uncertainty.

$j =$	$+$ (G_+)	$-$ (G_-)	$-$ (G_-), new α_c
a_{0j}	-0.00451760 ± 0.002	-0.00105483 ± 0.0008	-0.000519869 ± 0.0008
a_{1j}	0.0155766 ± 0.002	0.0157086 ± 0.0006	0.0153111 ± 0.0005
a_{2j}	0.422624 ± 0.2	0.345319 ± 0.05	0.356524 ± 0.05
a_{3j}	3.516054 ± 0.5	2.850094 ± 0.1	2.824663 ± 0.1
a_{4j}	1.015830 ± 0.04	0.935840 ± 0.02	0.927550 ± 0.02

see Figs. S12 and S13. At a very high density, $r_s = 0.1$ in Fig. S8, our model and the RA $G_+(r_s, q)$ exhibit very similar behaviors: a simple interpolation between small- and large-q asymptotics with a hump near $2k_F$. At a very low density, $r_s = 100$ in Fig. S9, our model tends to a smooth, hump-free interpolation between the two regimes, but the RA G_+ exhibits likely unphysical oscillations. This latter behavior of RA is consistent with its derivation from perturbation theory.

Moreover, from Figs. 1 and S1–S3, one can see that the QMC data validate the theoretically derived asymptotic expansions in the small-q limit, and are also consistent with the large-q limit. This is direct validation of the compressibility sum rule. All parameters in $G_+(r_s, q)$ are completely determined by r_s and the UEG correlation energy per electron.

Figure 2 plots the errors in the UEG correlation energies computed using this model and a few common approximations for G_+. The model of this work systematically overestimates the correlation energies, but makes errors comparable to any of the LFFs presented there. More accurate correlation energies require a frequency-dependent $G_+(r_s, q, \omega)$, such as those of Refs. [9–11]. The method of computation is described in Supplemental Material Sec. S5, and a validation of our method using the random phase approximation (RPA, $G_+^{\mathrm{RPA}} = 0$) is given in Supplemental Table S2.

Figure 3 compares our fitted G_- to the Kukkonen-Chen QMC data [13] for $r_s = 4$. The quality of fit is again excellent, lying within the QMC uncertainties at all points. The

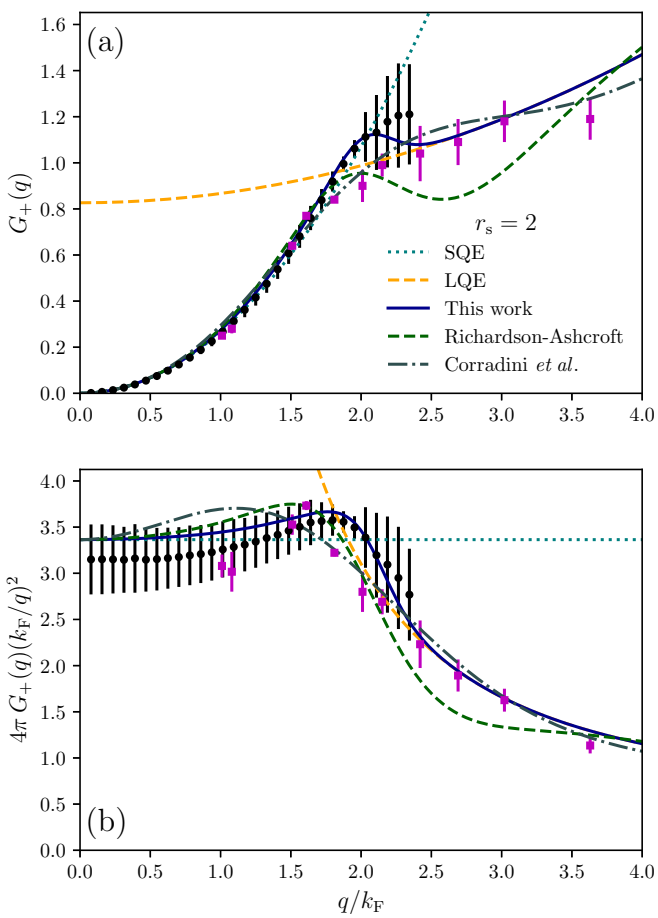

FIG. 1. Comparison of the model G_+ of Eq. (3) (blue, solid line) and Table I with the QMC data of Ref. [13] (black circles with vertical uncertainties) and [14] (magenta squares with vertical uncertainties) for $r_s = 2$. (a) presents G_+ and (b) $4\pi G_+(k_F/q)^2 = k_F^2 f_{xc}(q)$. The latter quantity, essentially the exchange-correlation kernel, is a sensitive test of the fit quality. Also shown are the LFFs of Corradini *et al.* [7] (gray, dashed-dotted), which is fitted to the data of Ref. [14], and of RA [9] (green, dashed). The small-q expansion (SQE) of Eq. (6) (teal, dotted) and large-q expansion (LQE) of Eq. (11) (orange, dashed) are also shown.

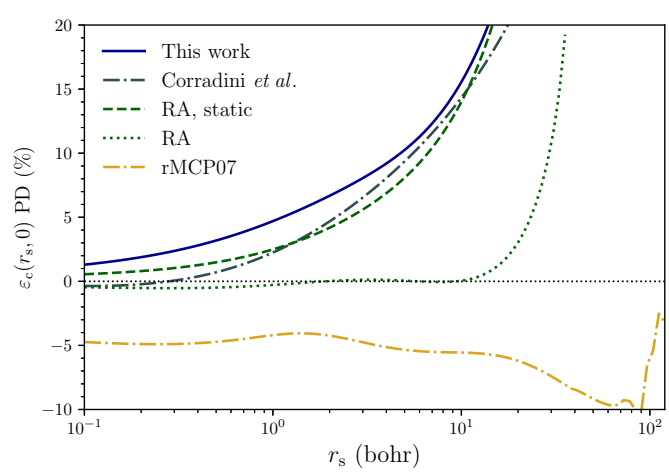

FIG. 2. Percent deviation (PD) from the Perdew-Wang approximation [28] of the UEG correlation energy, using a few common approximations for G_+. We define the PD as $(100\%)[1 - \varepsilon_c^{\mathrm{approx}}/\varepsilon_c^{\mathrm{PW92}}]$. The solid blue curve is computed using Eq. (3) and Table I. The dashed green curve is the static limit of the RA LFF [9], and the dotted green curve is its frequency-dependent form. The dashed-dotted gray curve is due to Ref. [7], and the dashed-dotted yellow curve to Ref. [11]. The numeric integration for both variants of the RA LFF appears to become unstable for $r_s \gtrsim 45$.

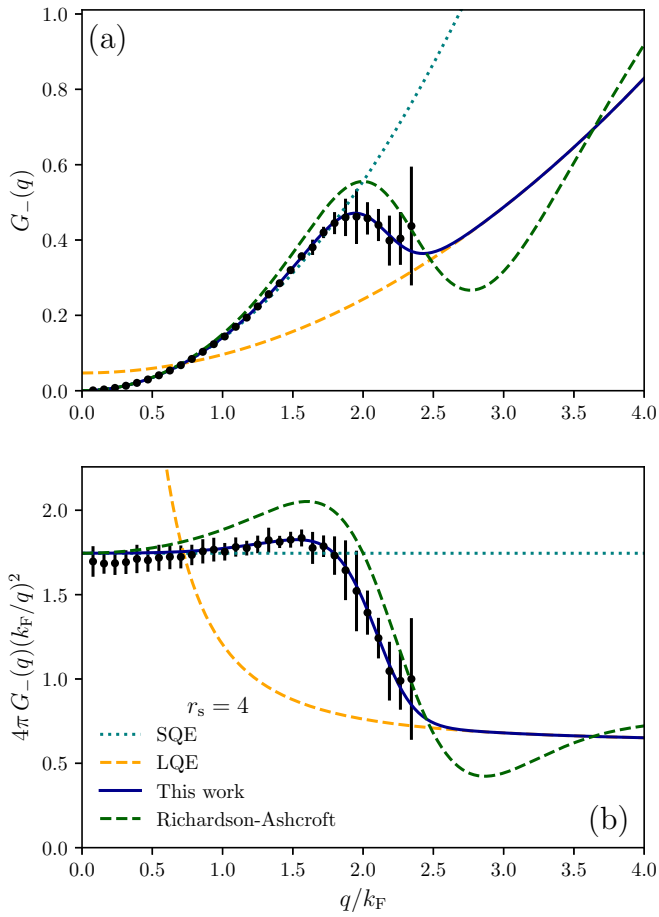

FIG. 3. Comparison of the model G_- of Eq. (3) (blue, solid curve) and Table I with the QMC data of Ref. [13] (black circles with vertical uncertainties) for $r_s = 4$. (a) presents G_- and (b) $4\pi G_-(k_F/q)^2$. The static RA [9] LFF is also shown (green, dashed). The small-q expansion (SQE) of Eq. (8) (teal, dotted) and the large-q expansion (LQE) of Eq. (14) (orange, dashed) are also shown.

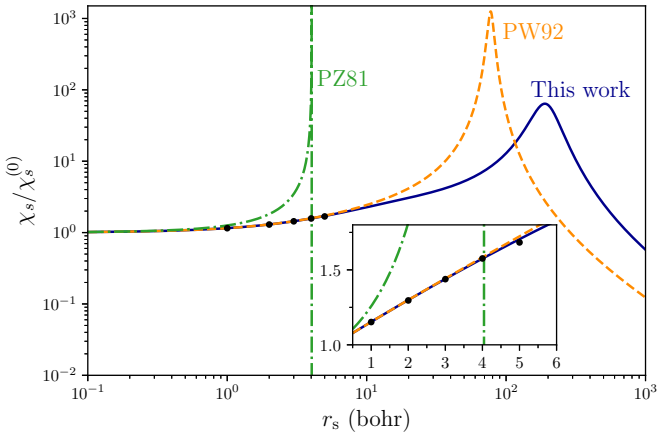

FIG. 4. Susceptibility enhancement $\chi_s/\chi_s^{(0)}$ computed with QMC [13,35] (black dots with almost imperceptible error bars), using Eq. (17) with the Perdew-Wang (PW92) [28] approximation for α_c (orange, dashed), the reparametrized form motivated here (blue, solid), or the older expression due to Perdew and Zunger (PZ81) [38] (green, dashed-dotted). Although PZ81 includes no explicit information on α_c, it is often used in solid-state and time-dependent density functional calculations. The inset shows the range $0.5 \leqslant r_s \leqslant 6$.

transition between small- and large-q asymptotics is apparent from Fig. 3(b). Equation (3) avoids the unusual oscillations present in the RA LFF, which is a rational polynomial in q^2.

Supplemental Figs. S4–S7 demonstrate the high quality of fit to $G_-(r_s, q)$ at other values of $r_s \in \{1, 2, 3, 5\}$. Extrapolations to the same high, $r_s = 0.1$, and low, $r_s = 100$, densities are made in Figs. S10 and S11, respectively. The same conclusions regarding G_+ hold for G_-: Our model and RA's are consistent at high densities, but RA's model becomes unphysically oscillatory at low densities. For surface plots of G_- at metallic densities, see Fig. S14.

These figures also show that the QMC data validate the asymptotic expansions of G_-, and thus the spin-susceptibility sum rule. Note that $G_-(r_s, q)$ depends on the parameters of $G_+(r_s, q)$ and the UEG on-top pair distribution function via Eq. (15).

Last, we discuss the accuracy of the PW92 parametrization of the correlation spin stiffness $\alpha_c(r_s)$. It can be observed from either Fig. 4 or Table S1 that the enhancement of the interacting spin susceptibility χ_s, over the noninteracting spin susceptibility $\chi_s^{(0)}$ (both per unit volume),

$$\frac{\chi_s}{\chi_s^{(0)}} = \left\{1 - \left(\frac{4}{9\pi}\right)^{1/3}\frac{r_s}{\pi} + 3\left(\frac{4}{9\pi}\right)^{2/3} r_s^2\alpha_c(r_s)\right\}^{-1}, \quad (17)$$

predicted by PW92 is not consistent with QMC calculations for $r_s > 10$ bohrs [13,35]. For all applications besides low-density jellium, extensive tests have shown PW92 to be robust. In units of the electron spin moment, $\chi_s^{(0)} = 3n/k_F^2$. Recent QMC calculations of $\chi_s/\chi_s^{(0)}$ and of the UEG correlation energy at low densities [36] make it possible to accurately fit α_c directly. The Perdew-Wang model of $\alpha_c(r_s)$ is

$$\alpha_c(r_s) = 2A(1 + \alpha_1 r_s) \times \ln\left[1 + \frac{1}{2A\left(\beta_1 r_s^{1/2} + \beta_2 r_s + \beta_3 r_s^{3/2} + \beta_4 r_s^2\right)}\right], \quad (18)$$

where A, β_1, and β_2 are constrained to ensure the analytic high-density expansion [30]

$$\lim_{r_s\to 0}\alpha_c(r_s) \approx -\frac{1}{6\pi^2}\ln r_s + 0.035\,474\,401. \quad (19)$$

We have recomputed the constant term. To refit α_c, we minimized the deviation from the tabulated values of the susceptibility enhancement [13,35], and from approximate values of the spin stiffness at low densities [36]. See Supplemental Material Sec. S1 for a description of this method. Table II presents fitted parameters and expansion coefficients. Our parametrization is recommended only for applications where a higher precision of $\alpha_c(r_s > 10)$ is needed: Our model and PW92 appear to differ at most by about 3.3% at $r_s = 18.3$ bohrs. We still use the PW92 parametrization of α_c in our model G_- via Eq. (9). Table I also provides model parameters for G_- using the current parametrization of α_c. Consistent

TABLE II. Left two columns: Parameters appearing in Eq. (18) for the correlation spin stiffness, $\alpha_c(r_s)$. Right two columns: Expansion coefficients derived using these parameters, such that $\lim_{r_s\to 0}\alpha_c(r_s) = c_0 \ln r_s - c_1 + c_2 r_s \ln r_s - c_3 r_s + \cdots$ and $\lim_{r_s\to\infty}\alpha_c(r_s) = -d_0/r_s + d_1/r_s^{3/2} + \cdots$.

α_c parameter		Expansion coefficient	
A	0.016886864	c_0	−0.016886864
α_1	0.086888870	c_1	0.035474401
β_1	10.357564711	c_2	0.001467281
β_2	3.623216709	c_3	0.005782963
β_3	0.439233491	d_0	0.210976870
β_4	0.411840739	d_1	0.225009568

with the improvements in α_c, the quality of fit is numerically improved, although the two variants of G_- are visually indistinct.

Consistent with recent QMC-driven analyses of the low-density phases of the UEG [36,37], our parametrization of α_c yields no divergence in the susceptibility enhancement. The present and PW92 parametrizations of α_c both predict near divergences in $\chi_s/\chi_s^{(0)}$. Such a divergence would indicate a ferromagnetic instability in the low-density UEG, whereby a transition from the paramagnetic to ferromagnetic fluid phases is possible. Both Refs. [36,37] find that a transition to a Wigner crystal phase occurs before a transition to the ferromagnetic fluid phase.

In summary, this Letter presents straightforward analytic models of the static density (spin-symmetric) and spin (antisymmetric) local field factors of the uniform electron gas (UEG), which are fitted to recent QMC data [13]. These models hold at an extremely wide range of densities, and the model of G_+ predicts UEG correlation energies with accuracy sufficient to recommend use in practical calculations of simple metallic systems. We have also reparametrized the correlation spin stiffness of the UEG using QMC data [13,35,36], which shows no transition to a ferromagnetic fluid phase.

A.D.K. thanks Temple University for support from a presidential fellowship. We acknowledge helpful discussions with John P. Perdew.

[1] G. F. Giuliani and G. Vignale, *Quantum Theory of the Electron Liquid* (Cambridge University Press, Cambridge, UK, 2005).
[2] J. Lindhard, Mat. Fys. Medd. Dan. Vid. Selsk. **28**, 1 (1954).
[3] E. Runge and E. K. U. Gross, Phys. Rev. Lett. **52**, 997 (1984).
[4] E. K. U. Gross and W. Kohn, Phys. Rev. Lett. **55**, 2850 (1985).
[5] A. Zangwill and P. Soven, Phys. Rev. A **21**, 1561 (1980).
[6] B. Farid, V. Heine, G. E. Engel, and I. J. Robertson, Phys. Rev. B **48**, 11602 (1993).
[7] M. Corradini, R. Del Sole, G. Onida, and M. Palummo, Phys. Rev. B **57**, 14569 (1998).
[8] Z. Qian and G. Vignale, Phys. Rev. B **65**, 235121 (2002).
[9] C. F. Richardson and N. W. Ashcroft, Phys. Rev. B **50**, 8170 (1994).
[10] A. Ruzsinszky, N. K. Nepal, J. M. Pitarke, and J. P. Perdew, Phys. Rev. B **101**, 245135 (2020).
[11] A. D. Kaplan, N. K. Nepal, A. Ruzsinszky, P. Ballone, and J. P. Perdew, Phys. Rev. B **105**, 035123 (2022).
[12] See Supplemental Material at http://link.aps.org/supplemental/10.1103/PhysRevB.107.L201120 for a detailed discussion of the fitting procedures; additional figures of the LFFs at densities for which they are fit, and at densities to which they extrapolate; surface plots of the current LFF compared to previous models; a discussion of the method of computation of correlation energies; and corrected expressions for the Richardson-Ashcroft LFFs.
[13] C. A. Kukkonen and K. Chen, Phys. Rev. B **104**, 195142 (2021).
[14] S. Moroni, D. M. Ceperley, and G. Senatore, Phys. Rev. Lett. **75**, 689 (1995).
[15] A. W. Overhauser, Phys. Rev. B **2**, 874 (1970), and references therein.
[16] K. Utsumi and S. Ichimaru, Phys. Rev. B **22**, 5203 (1980).
[17] Y. R. Wang, M. Ashraf, and A. W. Overhauser, Phys. Rev. B **30**, 5580 (1984), and references therein.
[18] J. J. Shirron and J. Ruvalds, Phys. Rev. B **34**, 7596 (1986).
[19] C. A. Kukkonen and A. W. Overhauser, Phys. Rev. B **20**, 550 (1979).
[20] T. Büche and H. Rietschel, Phys. Rev. B **41**, 8691 (1990).
[21] P. Virtanen, R. Gommers, T. E. Oliphant, M. Haberland, T. Reddy, D. Cournapeau, E. Burovski, P. Peterson, W. Weckesser, J. Bright, S. J. van der Walt, M. Brett, J. Wilson, K. J. Millman, N. Mayorov, A. R. J. Nelson, E. Jones, R. Kern, E. Larson, C. J. Carey *et al.*, Nat. Methods **17**, 261 (2020).
[22] W. H. Press, S. A. Teukolsky, W. T. Vetterling, and B. P. Flannery, *Numerical Recipes in Fortran 77* (Cambridge University Press, Cambridge, UK, 1992), pp. 686–687.
[23] M. Lein, E. K. U. Gross, and J. P. Perdew, Phys. Rev. B **61**, 13431 (2000).
[24] J. P. Perdew, A. Ruzsinszky, J. Sun, N. K. Nepal, and A. D. Kaplan, Proc. Natl. Acad. Sci. USA **118**, e2017850118 (2021).
[25] View the code repository at https://github.com/esoteric-ephemera/UEG_LFF, or the Python Package Index (PyPI) package at https://pypi.org/project/AKCK-LFF/. Both contain usage instructions, CC0 licensing information, and installation instructions.
[26] P. A. M. Dirac, Math. Proc. Cambridge Philos. Soc. **26**, 376 (1930).
[27] W. Kohn and L. J. Sham, Phys. Rev. **140**, A1133 (1965).
[28] J. P. Perdew and Y. Wang, Phys. Rev. B **45**, 13244 (1992).
[29] We use the most recent NIST CODATA for these values. Refer to https://physics.nist.gov/cgi-bin/cuu/Value?hr and https://physics.nist.gov/cgi-bin/cuu/Value?bohrrada0.

[30] S. H. Vosko, L. Wilk, and M. Nusair, Can. J. Phys. **58**, 1200 (1980).
[31] G. L. Oliver and J. P. Perdew, Phys. Rev. A **20**, 397 (1979).
[32] G. Niklasson, Phys. Rev. B **10**, 3052 (1974).
[33] X. Zhu and A. W. Overhauser, Phys. Rev. B **30**, 3158 (1984).
[34] J. P. Perdew and Y. Wang, Phys. Rev. B **46**, 12947 (1992).
[35] K. Chen and K. Haule, Nat. Commun. **10**, 3725 (2019).
[36] S. Azadi and N. D. Drummond, Phys. Rev. B **105**, 245135 (2022).
[37] M. Holzmann and S. Moroni, Phys. Rev. Lett. **124**, 206404 (2020).
[38] J. P. Perdew and A. Zunger, Phys. Rev. B **23**, 5048 (1981).